Water Resources Research

RESEARCH ARTICLE
10.1029/2020WR027392

Assessing the Steady-State Assumption in Water Balance Calculation Across Global Catchments

Juntai Han[1], Yuting Yang[1], Michael L. Roderick[2,3], Tim R. McVicar[3,4], Dawen Yang[1], Shulei Zhang[5], and Hylke E. Beck[6]

[1]State Key Laboratory of Hydroscience and Engineering, Department of Hydraulic Engineering, Tsinghua University, Beijing, China, [2]Research School of Earth Sciences, Australian National University, Canberra, Australian Capital Territory, Australia, [3]Australian Research Council Centre of Excellence for Climate Extremes, Canberra, Australian Capital Territory, Australia, [4]CSIRO Land and Water, Black Mountain, Canberra, Australia, [5]State Key Laboratory of Earth Surface Process and Resource Ecology, School of Natural Resources, Faculty of Geographical Science, Beijing Normal University, Beijing, China, [6]Department of Civil and Environmental Engineering, Princeton University, Princeton, NJ, USA

Key Points:
- The steady-state assumption in water balance calculation and associated errors across global catchments are assessed
- Arid/semiarid catchments require a longer time to reach an approximate steady state than humid/subhumid catchments
- Imbalance caused by ignoring storage change accounts for 7% (3%) of precipitation in arid (humid) catchments for a typical 10-year period

Supporting Information:
- Supporting Information S1

Correspondence to:
Y. Yang,
yuting_yang@tsinghua.edu.cn

Citation:
Han, J., Yang, Y., Roderick, M. L., McVicar, T. R., Yang, D., Zhang, S., & Beck, H. E. (2020). Assessing the steady-state assumption in water balance calculation across global catchments. *Water Resources Research*, *56*, e2020WR027392. https://doi.org/10.1029/2020WR027392

Received 22 FEB 2020
Accepted 25 JUN 2020
Accepted article online 29 JUN 2020

Abstract It has long been assumed that over a sufficiently long period of time, changes in catchment water storage (ΔS) are a relatively minor term compared to other fluxes and can be neglected in the catchment water balance equation. However, the validity of this fundamental assumption has rarely been tested, and the associated uncertainties in water balance calculations remain unknown. Here, we use long-term (1982–2011) observations of monthly streamflow (Q) and precipitation (P) for 1,057 global unimpaired catchments, combined with four independent evapotranspiration (E) estimates to infer ΔS and to provide a global assessment of the steady-state assumption in catchment water balance calculations. Results show that when the threshold for steady state is set to 5% of the mean monthly P, ~70% of the catchments attain steady state within 10 years while ~6% of the catchments fail to reach a steady state even after 30 years. The time needed for a catchment to reach steady state (τ_s) shows a close relationship with climatic aridity and vegetation coverage, with arid/semiarid and sparsely vegetated catchments generally having a longer τ_s. Additionally, increasing snowfall fraction also increases τ_s. The imbalance (e_{wb}) caused by ignoring ΔS decreases as averaging period for water balance calculations increases as expected. For a typical 10-year averaging period, e_{wb} accounts for ~7% of P in arid, but that decreases to ~3% of P in humid catchments. These results suggest that catchment properties should be considered when applying the steady-state assumption and call for caution when ignoring ΔS in arid/semiarid regions.

1. Introduction

Changes in catchment water storage (ΔS) consist of changes in the amount of water stored in both aboveground (e.g., river, lake, and snow) and belowground (unsaturated and saturated) water stocks. ΔS is also linked to catchment water outflow (i.e., surface runoff and groundwater flows) and governs numerous catchment ecohydrological processes (Flerchinger & Cooley, 2000; Rice & Emanuel, 2019; Yang et al., 2014, 2017). In the hydrologic community, it has long been assumed that over a sufficiently long period of time (e.g., annual or longer periods), ΔS is relatively minor when compared with the fluxes (i.e., precipitation, evapotranspiration, and runoff) averaged over the same period. Based on that assumption, it is common to neglect ΔS in the catchment water balance equation at the annual/mean-annual time scales (e.g., Koster & Suarez, 1999; Potter & Zhang, 2009; Xue et al., 2013; Yang et al., 2009). This is a fundamental assumption that underlies numerous catchment-based hydrologic studies, such as the estimation of catchment evapotranspiration (E) by subtracting runoff (Q) from precipitaton (P) (e.g., Donohue et al., 2007; Liang et al., 2015; Yang, Donohue, McVicar, Roderick, et al., 2016).

Despite its fundamental importance, the validity of the assumption that ΔS is negligible over some sufficiently long period is rarely evaluated. Thus, to examine the extent to which the steady-state assumption is valid and how it affects the water balance calculation, two key scientific questions need to be addressed: (i) How long does it take for a catchment to reach steady state (or near steady state), and (ii) how large is the error when the steady-state assumption is used for catchment-based water balance calculations.

A number of previous studies have assessed catchment ΔS at the annual time scale (e.g., Flerchinger & Cooley, 2000; Milly & Dunne, 2002; Rice & Emanuel, 2019; Wang, 2012; Wang et al., 2009). By using long-term soil moisture and groundwater observations, Wang (2012) quantified the interannual anomaly of ΔS in 12 catchments in Illinois, USA (ranging from 1,696 to 8,034 km^2), and found that the ratio of annual ΔS over annual P varied from −0.6 to 0.4, indicating that the proportion of storage change is too large to be neglected in annual water balance calculation in those catchments. Flerchinger and Cooley (2000) examined the annual water balance in a mountainous semiarid catchment (26 ha) in southwest Idaho, USA, and reported an average error of 46 mm year^{-1} when the steady-state assumption is applied, which was equivalent to ~10% of mean annual P and larger than mean annual Q (~30 mm year^{-1}) in that catchment. These findings suggest that for some catchments, the steady-state assumption is not valid at an annual time scale. In principle, as the integration time period increases, the variations in ΔS will become smaller relative to the integrated fluxes (Donohue et al., 2007; Liu et al., 2019; Zhang et al., 2008). Nevertheless, it is still unclear how long it takes for a catchment to reach a quasi-steady state such that the errors in the long-term mean water balance are small enough to be safely neglected.

The catchment water balance is primarily controlled by large-scale climate conditions, mediated by a number of local factors (Donohue et al., 2007; Istanbulluoglu et al., 2012; Milly, 1994; Roderick et al., 2014; S. Zhang et al., 2016; Zhang et al., 2018), which might also impact on the stability of catchment water storage. Precipitation (P) and potential evapotranspiration (E_P), respectively, represent water supply to and water demand from a catchment, the relative magnitude of which determines the long-term hydrological partitioning of the catchment (Budyko et al., 1974; Choudhury, 1999; Milly & Dunne, 2002; Yang et al., 2006, 2007; Zhang et al., 2004). Additionally, the temporal variability of P and E_P also exerts dominant control on the temporal dynamics of catchment water fluxes and water storage (Harman et al., 2011; Yin and Roderick, 2020; Yokoo et al., 2008). As for local factors, catchment area, water storage capacity, land cover, and vegetation are key factors in many hydrological processes (Harman et al., 2011; Li et al., 2013; Williams & Albertson, 2005; Yang et al., 2007; Yokoo et al., 2008). Catchment size directly determines the amount of precipitation and energy received by the catchment. Water storage capacity measures the maximum amount of water that can be held within a catchment. The partitioning of P into E generally increases with the increase of water storage capacity (Daly et al., 2019; Farmer et al., 2003; Koster & Suarez, 1999; Milly, 1994; Potter et al., 2005; Yin and Roderick, 2020). Vegetation, including both the aboveground (e.g., vegetation coverage or leaf area index) and belowground components (e.g., rooting depth), affects catchment hydrological partitioning primarily by increasing transpiration and enhancing infiltration, with direct consequences on root-zone soil water balance (Donohue et al., 2007, 2012; Llorens & Domingo, 2007; Wang et al., 2014; Yang, Donohue, McVicar, Roderick, et al., 2016). All the above factors are critical in controlling catchment hydrological processes, and the impacts of these factors on catchment water balance have been well documented previously. However, it still remains unknown how, and to what extent, these factors affect the variability of catchment water storage.

In this study, we use long-term (1982–2011) observations of monthly streamflow (Q) and precipitation (P) from 1,057 global unimpaired catchments. The observed P and Q are combined with four independent estimates of evapotranspiration (E) from global databases to infer ΔS. We then use the inferred time series of ΔS, to provide a comprehensive assessment of the steady-state assumption in water balance calculations using the catchment approach. The specific objectives are to (i) determine the time needed for a catchment to reach steady state; (ii) identify the factors controlling this time scale; and (iii) quantify errors in water balance calculations resulting from the steady-state assumption.

2. Materials and Methods

2.1. Determination of τ_s

For a given catchment, the water balance equation is given by

$$\frac{dS}{dt} = P - E - Q \tag{1}$$

where S is the catchment water storage (mm); t is time in month; and P, E, and Q are monthly precipitation (mm month^{-1}), evapotranspiration (mm month^{-1}), and runoff (mm month^{-1}), respectively. Note that

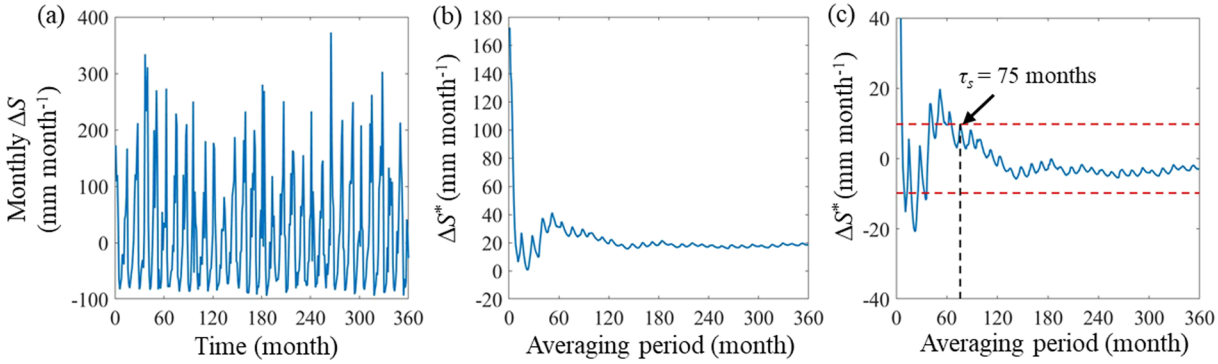

Figure 1. Example illustrating the determination of τ_s. (a) Time series of monthly storage change, (b) mean monthly storage change over an averaging period τ, and (c) mean monthly storage change over an averaging period τ after removing the systematic error. In (c), the dashed horizontal red lines represent the threshold when $k = 0.05$ (k is a proportion of mean monthly precipitation).

dS/dt represents changes in catchment water storage only when the catchment is a closed system (e.g., no lateral groundwater fluxes, but see Andréassian & Perrin, 2012). In the following analyses, all catchments are assumed to be closed systems as per the widely used assumption. With that in mind, integrating Equation 1 over time period τ, we have

$$\int_0^\tau \frac{dS}{dt}dt = \int_0^\tau (P - E - Q)dt \tag{2}$$

and it follows that

$$\frac{S_\tau - S_0}{\tau} = \frac{\Delta S}{\tau} = \Delta S^* = \overline{P} - \overline{E} - \overline{Q} \tag{3}$$

where ΔS (mm) is the total storage change during period τ (month) and ΔS^* is the mean rate of change of storage over the same period (mm month^{-1}). The bars above P, E, and Q represent the mean P, E, and Q (mm month^{-1}) over period τ.

Figure 1a shows an example of the monthly time series of dS/dt, and Figure 1b shows ΔS^* for τ varying from 1 to 360 months. In this example, it is clear that with the increase of τ, the fluctuations of ΔS^* gradually diminish with only a small seasonal oscillation, and in this example, the numerical value of τ is quasi-stable when τ exceeds ~180 months (or 15 years). In principle, when a catchment is at steady state, ΔS^* should strictly be zero. However, due to uncertainties in the other three water balance components (i.e., P, E, and Q), the observed ΔS^* may not be zero. In this particular example, ΔS^* stabilizes at a value around 20 mm month^{-1} when τ %3E ~180 months (Figure 1b). In this study, we consider the difference between ΔS^* over the entire analysis period and zero to be a systematic error (due to data uncertainties), which is further removed in the following analyses (Figure 1c). This procedure ensures that ΔS^* has the same reference value (i.e., zero) across all catchments.

We use a threshold to define the steady state. In practical applications, a steady state is often considered to be reached when ΔS^* is much smaller than the hydrological fluxes (i.e., P, E, and Q) (Donohue et al., 2007; Li et al., 2007; Roderick & Farquhar, 2011). Additionally, since a steady state is reached when the total input (i.e., P) equals the total output (i.e., $E + Q$), we define the threshold for establishing when steady state is reached using a fixed fraction (k) of mean monthly P over the entire analysis period. The time at which the steady state is first reached, denoted τ_s, is defined as the month when ΔS^* enters the interval defined by the threshold for the last time (Figure 1c). This procedure ensures that when τ %3E τ_s, $|\Delta S^*|$ is always smaller than the defined threshold. For the example used here (Figure 1c), ΔS^* falls into the interval set by the threshold at the 75th month and remains within that interval for the remaining period (Figure 1c). So τ_s for the example catchment is 75 months, as represented by the dashed black vertical line in Figure 1c.

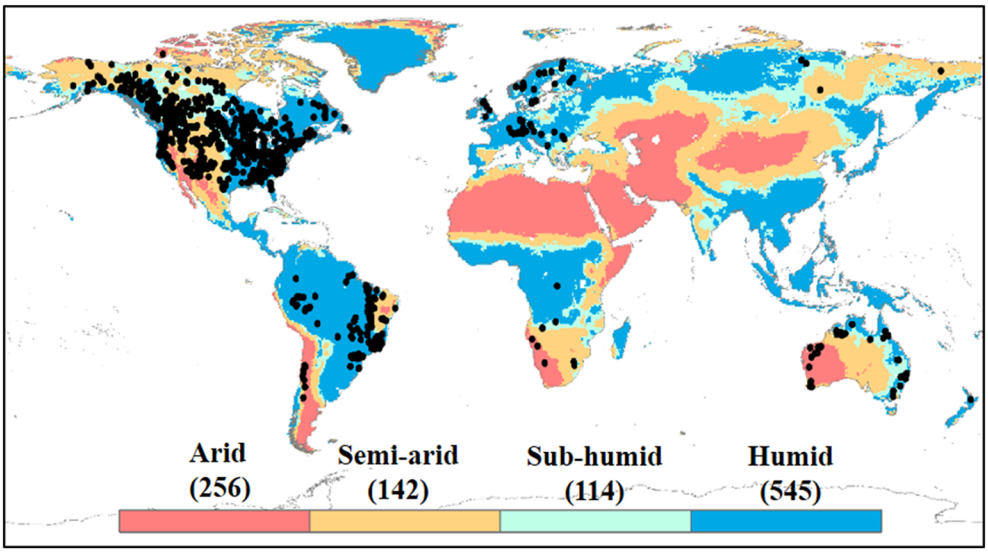

Figure 2. Location of the catchment used herein. The background shows the global dryness zones. The number of catchments in each of the four global dryness zones is provided in parenthesis. Global dryness zones are defined according to their dryness index (E_p/P): (i) arid (E_p/P %3E 1.35); (ii) semiarid (1.35 %3E E_p/P %3E 1); (iii) subhumid (1 %3E E_p/P %3E 0.76); and (iv) humid (E_p/P %3C 0.76) (McVicar et al., 2012), where E_P is potential evapotranspiration as per the CRU TS v. 4.03 data set (Harris et al., 2014).

2.2. Data

Daily Q observations at 21,868 catchments across the globe were obtained from six sources: (i) Global River Discharge Centre (http://www.bafg.de/GRDC; Lehner, 2012), (ii) the U.S. Geological Survey (USGS) National Water Information System (NWIS; https://waterdata.usgs.gov/nwis) and GAGES-II database (Falcone et al., 2010), (iii) the Australian Bureau of Meteorology (http://www.bom.gov.au/waterdata; Zhang et al., 2013), (iv) the Brazilian Agência Nacional de Águas (http://www.snirh.gov.br/hidroweb), (v) the Water Survey of Canada Hydrometric Data (HYDAT; https://www.canada.ca/en/environment-climate-change), and (vi) the Chilean Center for Climate and Resilience Research (CR2; http://www.cr2.cl/datos-de-caudales/). A number of selection criteria were used to ensure that only larger catchments with a continuous streamflow record, and with minimal human impact, were used. First, catchments with %3E5% missing data and any gaps longer than 10 days from 1 January 1982 to 31 December 2011 (30 years or 360 months) were removed. For catchments passing these criteria, gaps were filled in the remaining daily Q series using linear interpolation. Second, due to the coarse-resolution E data (see below descriptions for the four E data sets), catchments smaller than 2,500 km^2 (~0.5° × 0.5°) were excluded. Third, and finally, to ensure we only selected catchments with minimal disturbance, we excluded catchments with (i) irrigated areas larger than 3% of the total catchment area (based on the Global Map of Irrigation Areas-GMIA; Siebert et al., 2015); a 3% threshold is chosen as a compromise between data quality and the sample size, (ii) urban areas larger than 1% (based on the GlobCover v2.3 map; https://www.edenextdata.com/?q=data) and (iii) catchments with large dams whose reservoir capacity was larger than 10% of the mean annual Q (based on the Global Reservoir and Dam database v1.1; Lehner et al., 2011). A total of 1,057 catchments passed the above selection criteria and were used herein (Figure 2).

Three-hourly precipitation data at 0.1° spatial resolution from 1979 to 2017 was derived from the Multi-Source Weighted-Ensemble Precipitation (MSWEP) Version 2 data set, which represents an optimal combination of the highest quality P data sources available as a function of time scale and location (Beck et al., 2019). Precipitation on days with a daily mean air temperature lower than 1°C is considered to be snowfall (Berghuijs et al., 2014). Other climate variables, including daily air temperature and monthly E_P at 0.5° spatial resolution, were obtained from the WFDEI meteorological forcing data set (Weedon et al., 2014) and the CRU TS v. 4.03 data set (Harris et al., 2014), respectively. Actual evapotranspiration was derived using four global E data sets, including (i) the global monthly half-degree E estimates using the Penman-Monteith-Leuning (PML) model over 1982–2012 (E_{PML}; Y. Zhang et al., 2016); (ii) the global monthly

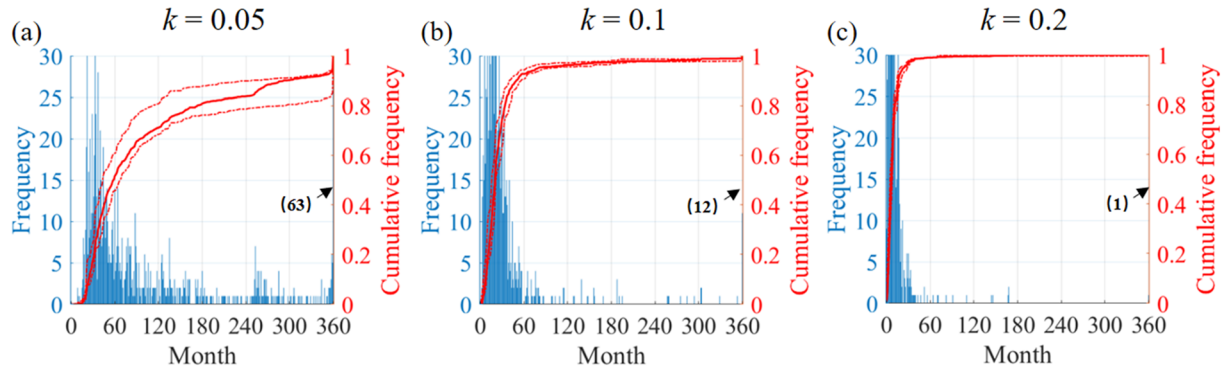

Figure 3. Histogram and the cumulative frequency distribution of τ_s across the 1,057 catchments using three different thresholds, (a) $k = 0.05$, (b) $k = 0.1$, and (c) $k = 0.2$. The red solid curves represent the mean τ_s determined from the three closest evapotranspiration products, and the red dashed curves are the maximum and minimum τ_s using the three evapotranspiration products. Numbers in the bracket show the number of catchments with τ_s longer than 360 months.

8 km^2 E estimates from the Process-based Land Surface Evapotranspiration/Heat Fluxes algorithm (P-LSH) over 1982–2013 ($E_{\text{P-LSH}}$; Zhang et al., 2015); (iii) the global monthly 0.25°E estimates from the Global Land Evaporation Amsterdam Model (GLEAM) Version 3.3 over 1980–2018 (E_{GLEAM}; Martens et al., 2017; Miralles et al., 2011); and (iv) the global monthly half-degree reconstructed E based on site level observations and an adaptive machine learning approach over 1982–2011 (E_{MTE}; Jung et al., 2011). All gridded data were aggregated and lumped for individual catchments at a monthly time scale. To quantify τ_s, we calculated τ_s using P, Q, and the four separate E estimates and determined the final τ_s as the mean of the three closest τ_s estimates for each catchment. This procedure excludes the most uncertain E estimates and improves the quality of E for each individual catchment. Following this approach, no particular E database was favored with E_{PML}, $E_{\text{P-LSH}}$, E_{GLEAM}, and E_{MTE} used in 833, 782, 777, and 779 of the 1,057 catchments, respectively.

To investigate the factors controlling τ_s across catchments, we also collected a series of catchment property data. Soil water holding capacity at a spatial resolution of 5 arc-minutes (~0.083°) was obtained from the Global Gridded Surfaces of Selected Soil Characteristics data set (Global Soil Data Task Group, 2000). Vegetation coverage is represented by the satellite-derived Normalized Difference Vegetation Index (NDVI), which was acquired from the half-monthly, 8 km^2 spatial resolution AVHRR GIMMS-3g global NDVI data sets covering 1982–2016 (Pinzon & Tucker, 2014). To determine catchment storage capacity (S_{max}), because observations of S_{max} is currently not available, we estimated S_{max} by assuming that S_{max} approximates the difference between the maximum and minimum storage during the study period for each catchment (Yin & Roderick, 2020). The catchment water storage at each monthly time step was calculated by first assuming zero storage at the beginning of the study period. Note that the resultant S_{max} may be smaller than the physical storage capacity of a catchment, since under real conditions, a zero storage can hardly be met for catchments even after prolonged droughts. Indeed, the S_{max} estimated using the above method is better thought of as an "effective storage capacity"—the water stored that is actively participating in the hydrological cycle. Consequently, we denote S_{max} as the effective storage capacity in the following text.

3. Results

3.1. Spatial Distribution of τ_s

The time when the steady state is reached under different thresholds (by varying the coefficient k) across the 1,057 catchments is shown in Figure 3. Under the tightest condition (i.e., $k = 0.05$), about 80% of the catchments attain a quasi-steady state within ~180 months (or 15 years), and this fraction reduces to 71% and 53% when the steady state is reached within 120 and 60 months (corresponding to 10 and 5 years), respectively (Figure 3a). In addition, there are 63 catchments for which a steady state was not reached within the study period (i.e., τ_s %3E 360 months). τ_s becomes shorter when the threshold is relaxed to $k = 0.1$ and $k = 0.2$, at which ~97% and ~99% of the catchments reach the steady state within 10 years, respectively (Figures 3b and 3c). Nevertheless, there are still 12 catchments requiring τ_s longer than 30 years for the threshold of $k = 0.1$ and 1 catchment for the $k = 0.2$ threshold. Catchments with a long τ_s are generally found in relatively cold (e.g., high latitudes) and/or very dry regions (e.g., the western United States, the Brazilian Highlands,

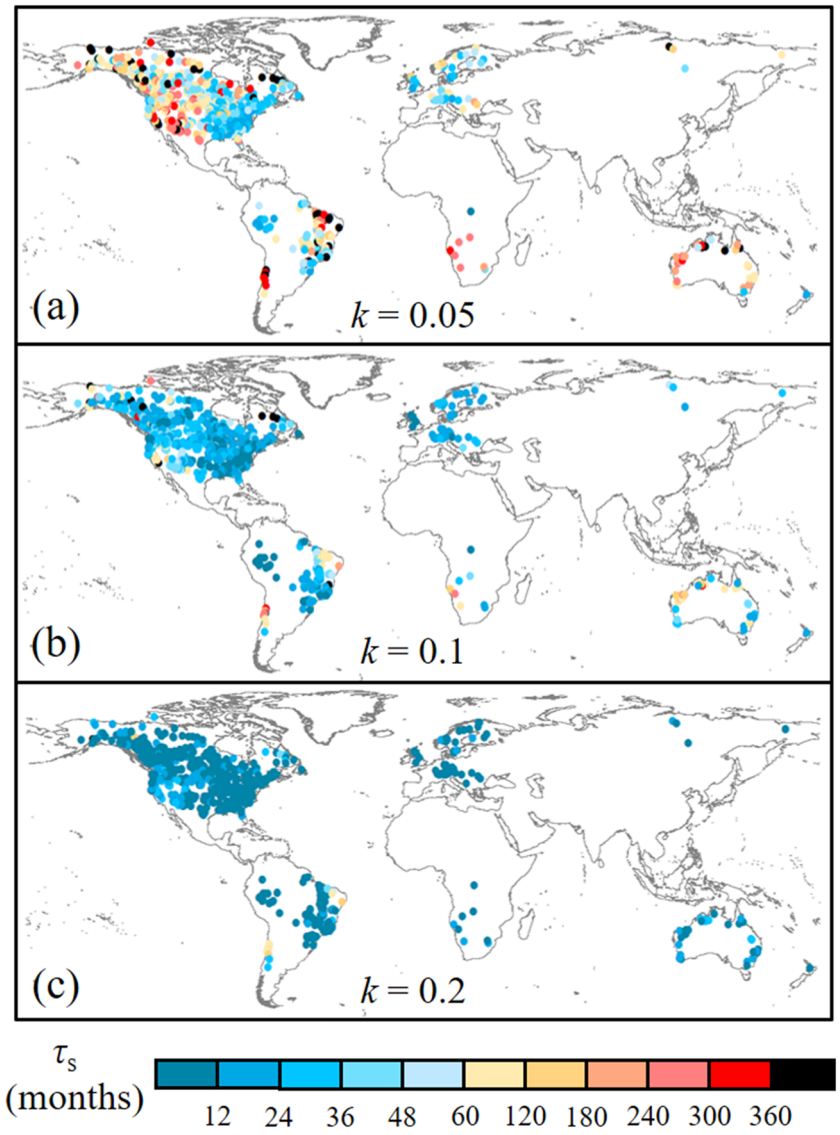

Figure 4. Spatial distribution of τ_s. The spatial distribution of τ_s using the three thresholds, (a) $k = 0.05$; (b) $k = 0.1$, and (c) $k = 0.2$.

Southern Africa, and Western Australia), whereas catchments with short τ_s are mostly concentrated in humid eastern United States, Europe, and Amazonia (Figure 4a). Averaged over all catchments (excluding catchments with τ_s longer than 30 years), the mean τ_s ($\pm$1 sd) is 116 $\pm$ 8, 28 $\pm$ 2, and 10 $\pm$ 1 months for the $k = 0.05$, $k = 0.1$, and $k = 0.2$ thresholds, respectively. Similar results were achieved when different initial years (e.g., 1982, 1983, or 1984) were used to the define the study period (Figure S1 in the supporting information). Results were also similar using annual instead of monthly fluxes to estimate τ_s (Figure S2). For example, the mean τ_s using annual fluxes was 9.1 years compared to 116 months (or 9.8 years) based on monthly fluxes.

3.2. Factors Controlling τ_s

To further understand the spatial pattern of τ_s and explore the factors that control the steady-state time scale, we conducted a series of regression analyses between τ_s and various climate factors/surface properties (Figures 5–7). Only results for $k = 0.05$ (closest to the theoretical steady state, $\Delta S^* = 0$) are provided here. For climate factors, τ_s typically increases as the climate becomes drier. Mean τ_s increases rapidly from 69 months (or ~6 years) in humid catchments to 188 months (~16 years) in arid catchments (Figure 5a).

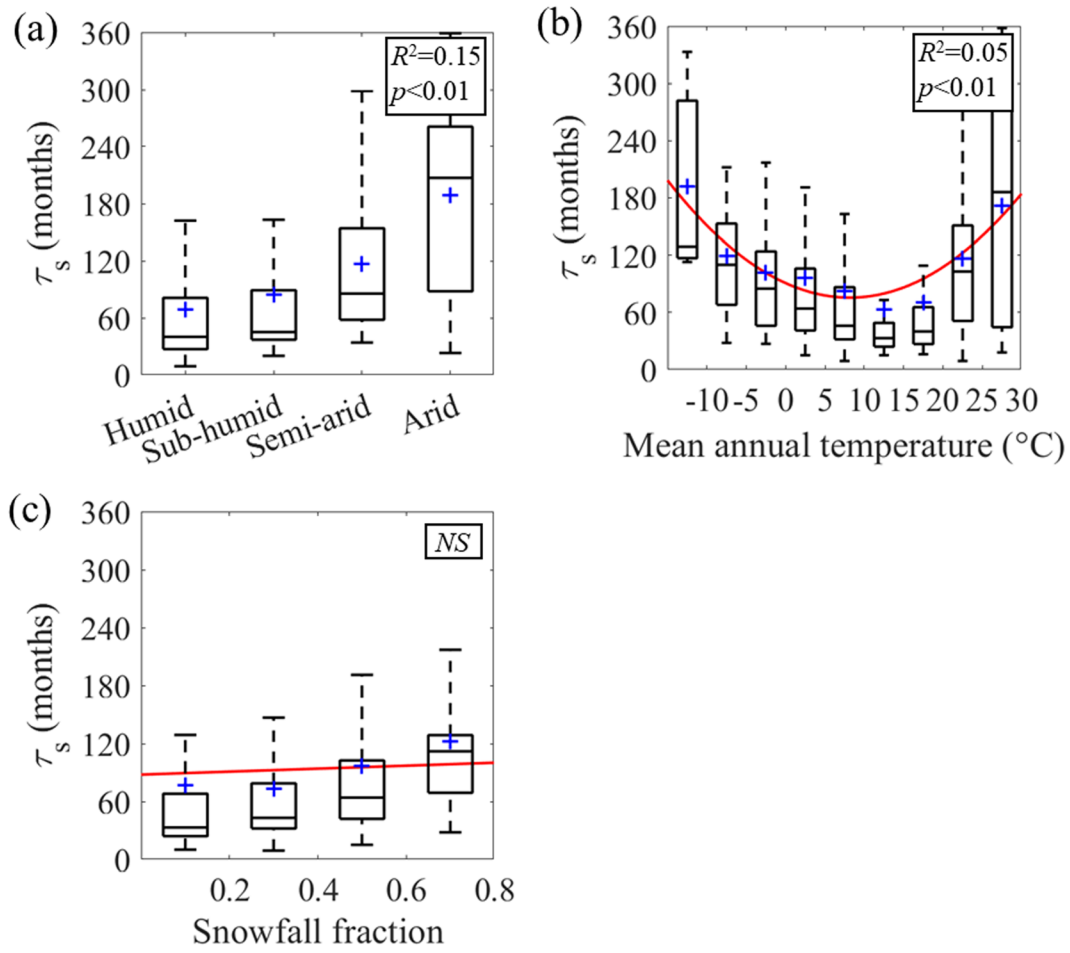

Figure 5. Relationship between τ_s and (a) dryness zones, (b) mean annual air temperature, and (c) mean annual snowfall fraction. In all plots the whiskers represent the maximum and minimum value, the top and bottom of the box are the 25th and 75th percentile, and the median is represented by the horizontal line and the mean by the blue plus sign. For (b) and (c) the red line shows the best fit relationship. The regressions are performed across all 1,057 catchments. Also, shown are the coefficient of determination (R^2) and the significance of the relationship (p value), with *NS* indicated no significance relationship.

In contrast, air temperature exhibits a quadratic relationship with τ_s, with the shortest τ_s generally found in catchments with a mean annual air temperature of 10–15°C (Figure 5b), whereas no significant relationship is found between τ_s and the catchment snowfall fraction (i.e., the fraction of precipitation falling as snow) (Figure 5c). Nevertheless, if we only considered catchments with a snowfall fraction higher than 10% (744 catchments), τ_s shows a significant (at 99% significance level calculated with an F test) positive relationship with snowfall fraction, that is, a higher snowfall fraction corresponds to a longer τ_s (Figure 6b). Since a higher snowfall fraction is often associated with a lower temperature (Figure S3), the above-noted positive τ_s-snowfall fraction relationship also concurs with the negative relationship between τ_s and air temperature in cold regions. In addition, the negative τ_s-temperature relationship also becomes stronger when focusing on catchments having a snowfall fraction higher than 10% (Figure 6a).

For the four surface properties investigated here, τ_s shows a strong negative relationship with vegetation coverage (represented by NDVI; Figure 7a) and a weak positive (yet statistically significant) relationship with catchment effective storage capacity (S_{max}; Figure 7b). In addition, no significant relationship is found between τ_s and catchment size nor between τ_s and soil water holding capacity (Figures 7c and 7d). Since S_{max} of a catchment is also partly dependent on soil water holding capacity, the above results imply that S_{max} is actually more determined by soil depth than the capacity of a unit depth of soil to hold water.

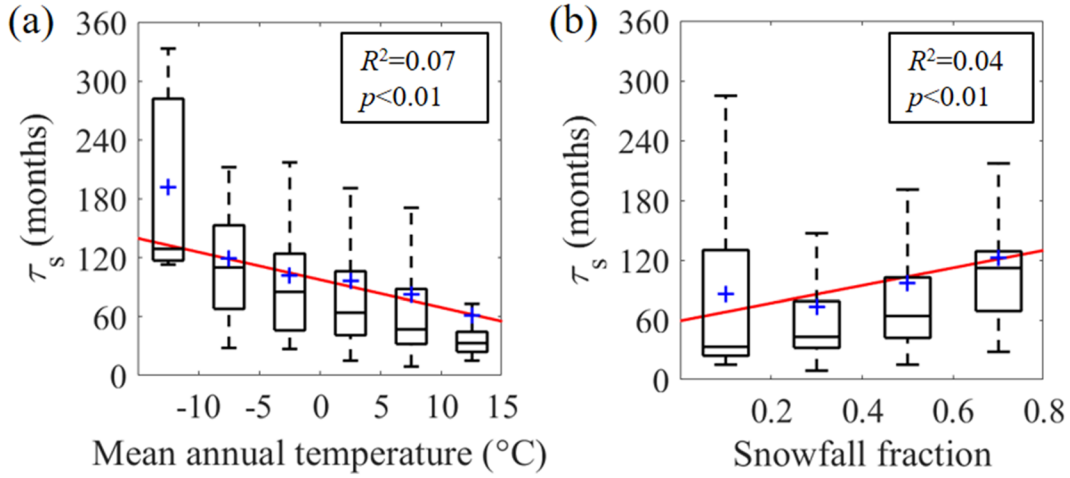

Figure 6. Relationship between τ_s and (a) mean annual air temperature, (b) mean annual snowfall fraction for catchments with mean annual snowfall fraction higher than 10%. The regressions are performed across 744 catchments with mean annual snowfall fraction higher than 10%. Also shown are the coefficient of determination (R^2) and the significance of the relationship (p value).

3.3. Imbalance in Catchment Water Balance Calculations Under a Steady-State Assumption

We next quantify the long-term imbalance in the catchment water balance calculation (at annual/mean-annual scales as widely used in existing studies) as a result of the steady-state assumption, that is, the residual in the water balance calculation when assuming a zero storage change (e_{wb}). To enable comparisons across catchments, we normalize the absolute e_{wb} (mm year^{-1}) to mean annual P, E, and Q, respectively, for each catchment. Figure 8 depicts the distribution of e_{wb}, as a fraction of mean annual P, E, and Q within the space defined by τ_s (under $k = 0.05$) and the time scale at which the water balance calculation is performed (τ_{wb}). In all three plots, there is a clear divide around the 1:1 line and larger e_{wb} are found in the bottom right corner of the τ_s-τ_{wb} space, where the catchments require a longer time to reach steady state but the water balance calculation is performed at a shorter time scale. The magnitude of imbalance increases as the positive difference between τ_s and τ_{wb} increases and decreases when the difference between τ_s and τ_{wb} becomes more negative. In general, when τ_s %3C τ_{wb}, e_{wb} is smaller than 4% of mean annual P and 7% of mean annual E but can reach as high as ~80% of mean annual Q, respectively. However, when τ_s %3E τ_{wb}, e_{wb} can be up to 15% of mean annual P, 19% of mean annual E, and 143% of mean annual Q. Note that these numbers are average e_{wb} among catchments within each τ_s-τ_{wb} category; e_{wb} in individual catchment can be much larger than that.

To give a further idea of how e_{wb} varies across catchments, we group the catchments according to their climate dryness and perform the steady-state water balance calculation at 1-, 3-, 5-, and 10-year periods. These four periods were chosen because they are often used in existing water balance calculations for a variety of catchment-based studies. Despite an increasing e_{wb} with the decrease of τ_{wb} as reported above, e_{wb} also shows a notable gradient with climate dryness, with larger e_{wb} generally found in more arid catchments (Figure 9). This is not surprising since τ_s also increases as the climate becomes drier (Figure 5a). In humid and subhumid catchments, on average, e_{wb}, respectively, accounts for less than 5% and 10% of mean annual P and mean annual E when the water balance calculation is performed at time scales longer than 3 years. For arid catchments, e_{wb} can account for more than 5% of mean annual P, and e_{wb}/E still remains about 5% to 10% when τ_{wb} is longer than 3 years. A much larger contrast is found for e_{wb}/Q along the climate dryness gradient (Figures 9e–9h). For a typical 10-year mean, e_{wb}/Q is ~5.5% for humid catchments and skyrockets to ~100% for arid catchments.

4. Discussion

The steady-state assumption refers to the assumption of negligible storage change that is widely used to undertake catchment-based water balance calculations for many hydrological applications. To our

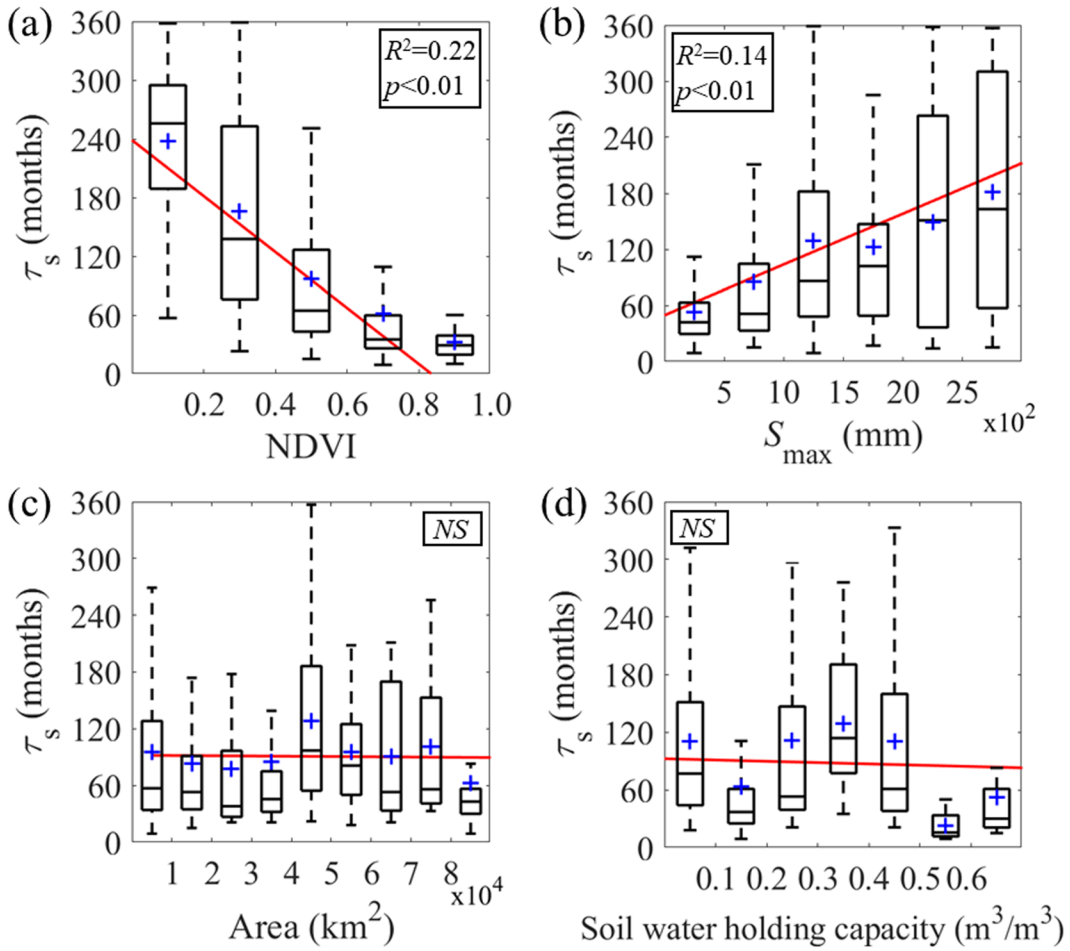

Figure 7. Relationship between τ_s and surface properties for all 1,057 catchments. Relationship between τ_s and (a) NDVI, (b) effective storage capacity, (c) catchment area, and (d) soil water holding capacity. Whiskers represent the maximum and minimum value, the top and bottom of the box are the 25th and 75th percentile, and the median represented by the horizontal line and the mean by the blue plus sign. The red line provides the line of best fit. The regressions are performed across all 1,057 catchments. Also shown are the coefficient of determination (R^2) and the significance of the relationship (p value), with *NS* indicated no significance relationship.

surprise, such an important assumption has never been formally assessed globally although assessments have been made for specific catchments/regions (Donohue et al., 2010; Flerchinger & Cooley, 2000; Rice & Emanuel, 2019; Wang, 2012; Zhang et al., 2008). By combining observations of catchment streamflow and precipitation with satellite/machine learning-based evapotranspiration estimates, for the first time, we assessed the utility of the steady-state assumption across global catchments covering a broad range of bioclimates. We find that many catchments assessed here do not reach the steady state within a decade or even over a 30-year period (Figures 3 and 4), which is well beyond an often assumed 1- to 5- to 10-year period adopted in many existing studies (Evans & Jakeman, 1998; Greve et al., 2016; Li et al., 2007; Potter & Zhang, 2009; Xue et al., 2013; Yang et al., 2009; Yang, Donohue, & McVicar, 2016).

4.1. Factors Determining τ_s

In practice, two key factors determine τ_s for a catchment, being (i) the temporal variability of ΔS and (ii) the magnitude of ΔS relative to the hydrological fluxes (i.e., the threshold in Figure 1c). Previous studies have shown that the coefficient of variation of P is generally higher in dry regions and steadily decreases as the climate becomes wetter (Monteverdi, 1976; Le Houérou et al., 1988; also see Figure S4). However, a higher coefficient of variation for P does not necessarily lead to a higher coefficient of variation of ΔS; the variability of ΔS also depends on the partitioning of the variance in P into the variance in ΔS. Using global hydrological reanalysis, Yin and Roderick (2020) found that the fraction of P variance partitioned into ΔS variance is

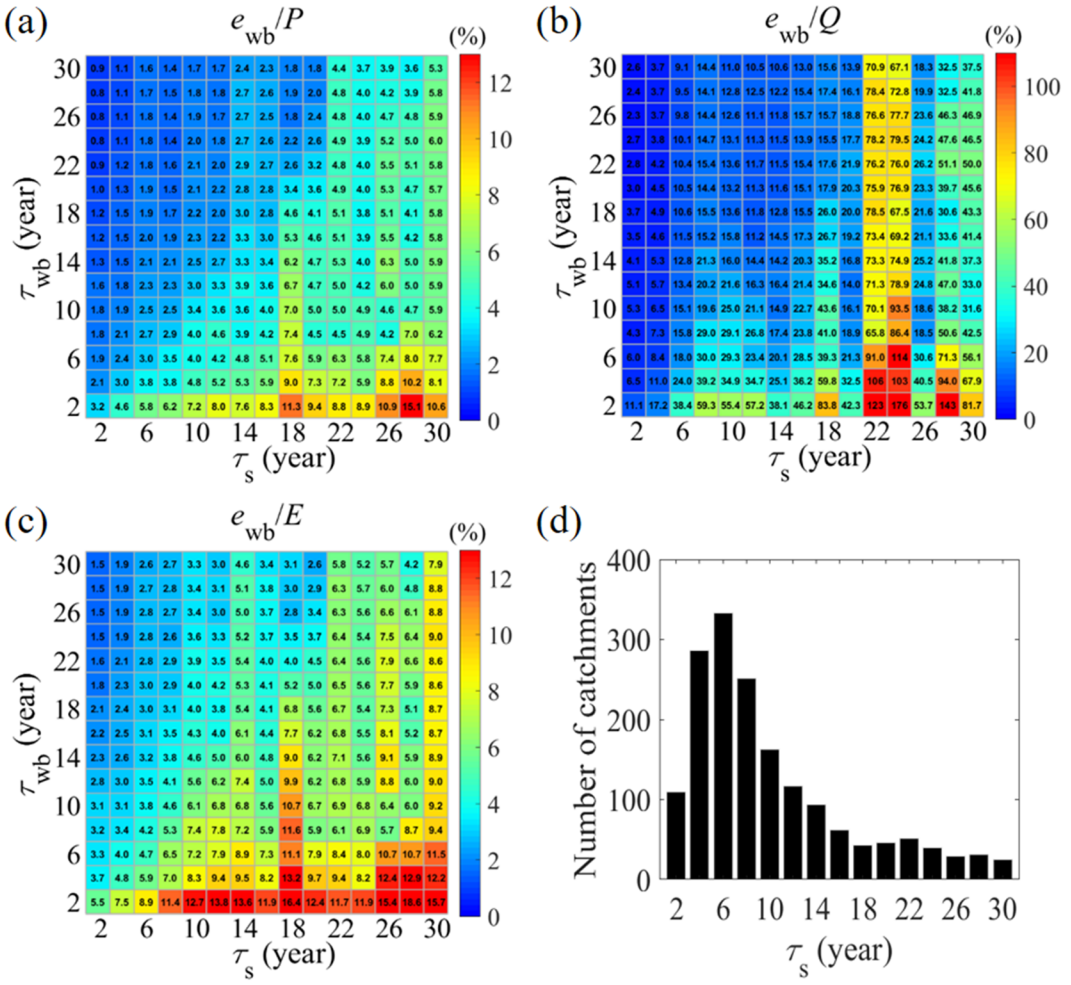

Figure 8. Imbalance in catchment water balance calculation as a result of the steady-state assumption (e_{wb}). The magnitude of imbalance is expressed as a fraction of (a) mean annual precipitation (P), (b) mean annual runoff (Q), and (c) mean annual evapotranspiration (E). The value in each τ_s-τ_{wb} grid represents the average imbalance over all catchments with τ_s and τ_{wb} that fall in each grid; the number of catchments for each τ_s category is shown in (d). The ranges of both τ_s and τ_{wb} are 0–30 years, with an interval of 2 years. For example, the top right grid (30, 30) represents catchments with a τ_s of 29–30 years while the water balance calculation is performed at the 30-year scale.

generally small in humid regions, medium in arid regions, and highest in semiarid regions where mean annual P equals mean annual E (also see Figure S5). This, together with a higher coefficient of variation in P in arid regions, largely explains the long τ_s in both arid and semiarid catchments but a much shorter τ_s in humid catchments (Figure 5a).

In addition to the overall positive climate dryness-τ_s relationship, we find that snowfall fraction and vegetation coverage also show evident relationships with τ_s, with a longer τ_s found in catchments with a higher snowfall fraction and/or lower green vegetation cover (Figure 5c, 6b, and 7a). When snowfall occurs, the precipitation contributes to a temporary catchment storage that is released upon melting and leads to higher ΔS variability and consequently a longer τ_s (Figures 5c, 6b, and S6). As for vegetation, since the spatial pattern of vegetation cover largely follows that of climate dryness (vegetation coverage is low/high in arid/humid regions; Yang et al., 2015), it is not surprising that τ_s shows a significant negative relationship with NDVI (Figure 7a). Apart from the coevolution between vegetation and climate, vegetation itself may also play a role in determining τ_s by modifying the partitioning of P and its variability into E, Q, ΔS, and the corresponding variance components. Yin and Roderick (2020) also found that the ratio of ΔS variance over P variance is highest when the mean annual E more or less equals the mean annual P where vegetation also tends to show the largest rooting depth (Yang, Donohue, McVicar, Roderick, & Beck, 2016), suggesting a higher root zone

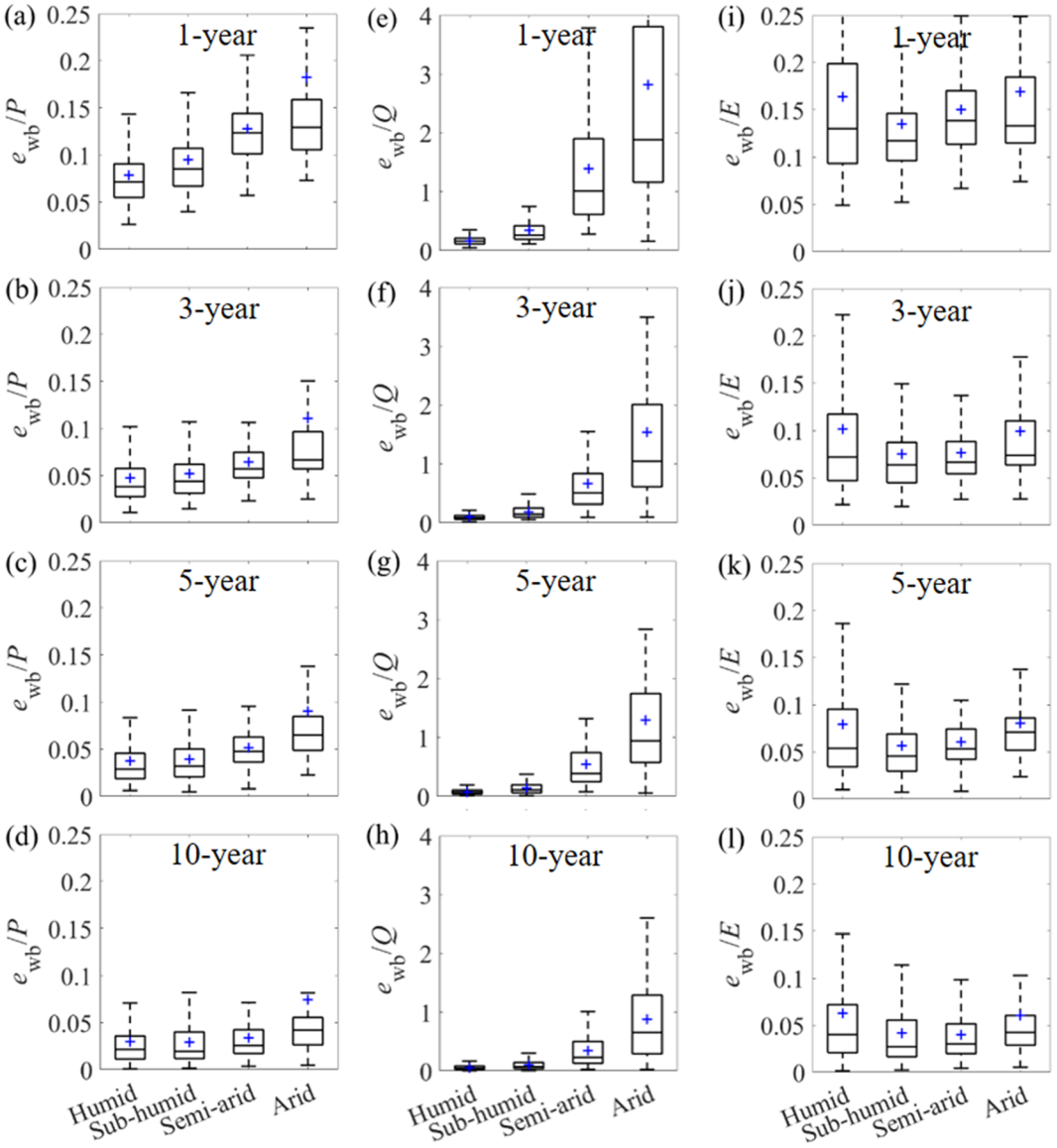

Figure 9. Imbalance in the catchment water balance as a result of the steady-state assumption in different climatic regions. The magnitude of the imbalance is expressed as a fraction of (a–d) mean annual P; (e–h) mean annual Q; and (i–l) mean annual E. Whiskers represent the maximum and minimum value, the top and bottom of the box are the 25th and 75th percentile, and the mean is represented by the horizontal line and the median by the blue plus sign. The number of catchments in each of the four global dryness zones is provided in Figure 2.

soil water storage capacity. As a result, a higher fraction of P variance being partitioned into ΔS variance in deeply rooted catchments may partly explain the positive relationship between τ_s and S_{max} (Figure 7b). Another possible explanation is that a higher vegetation cover is able to maintain a more steady return flow of water from the soil to the atmosphere, thereby minimizing variations in storage change within the root zone (Anderegg et al., 2016; Emanuel et al., 2007, 2014; Nippgen et al., 2015, 2016; Rice & Emanuel, 2019).

4.2. Imbalance in Water Balance Calculation as a Result of the Steady-State Assumption

Our above analyses (Figures 8 and 9) clearly demonstrate an imbalance usually occurs when the steady-state assumption is used for catchment water balance calculations. This imbalance is in practical hydrologic terms, a modeling error. In that light, we find that larger relative errors are always associated with Q estimation, especially in arid and semiarid catchments (Figures 8b and 9e–9h). This is primarily due to a relatively

small Q in drier regions (Abatzoglou & Ficklin, 2017; Beck et al., 2015; Peel et al., 2010). In contrast, in similar arid and semiarid catchments, the ratio of e_{wb} over E is typically lower than 10% when the water balance calculation is performed at a 5-year period or longer (Figures 8c and 9l). The implication is that by using a 5-year period (or longer), using the water balance equation to estimate E while ignoring storage change would only incur errors less than 10%. Additionally, we find that the relationship between e_{wb}/E and climate dryness does not simply follow a wet/low e_{wb}/E-dry/high e_{wb}/E gradient as we found for e_{wb}/P and e_{wb}/Q; e_{wb}/E is higher in both humid and arid catchments but slightly lower in semiarid and subhumid catchments (Figures 9i–9l). This is because in arid climates, the lower water availability constrains E, and in humid climates, the available energy, which can be low in wet and cold environments, constrains E (see Figure S7). Consequently, water and energy constraints respectively limit the magnitude of E to a relatively small value in dry and wet (and cold) environments and thus resulting in a higher e_{wb}/E in both arid and humid catchments.

4.3. The Threshold for Determining τ_s

The determination of τ_s is subject to the chosen threshold. In this study, we compare changes in storage with the fraction of mean monthly P, considering that a theoretical steady state is reached when the total input equals the total outputs. However, in real hydrological applications, E and/or Q are often of more practical interest. In this light, using E or Q to define the threshold may also be reasonable. In the supporting information, we test alternate formulations by setting the threshold as a fixed fraction of the minimum of mean monthly E and Q. Despite a general longer τ_s (due to a narrower threshold band), τ_s determined from E/Q threshold shows very consistent relationships with catchment climatic factors and surface properties as τ_s as when using a P threshold, suggesting that the use of different thresholds would not materially change the spatial pattern of τ_s and its dependence on environmental factors (Figures S8–S12). In addition, the error as a result of the steady-state assumption in water balance calculation across global dryness zones shown in Figure 9 does not depend on either τ_s or the threshold of determining τ_s, which provides a robust suggestion on the error-oriented selection of the time period at which a steady-state assumption may be applied.

4.4. Implications and Limitations

Using the water balance equation to estimate catchment Q and/or E while ignoring storage change at the mean-annual scale has long been used in practical applications by the hydrological community. One of the most common data-based approaches is to use observed P and Q to determine long-term catchment E while ignoring storage change (e.g., Peel et al., 2010; Ukkola & Prentice, 2013; Xue et al., 2013; Yang, Donohue, & McVicar, 2016). In addition, recent developments of global hydrological reanalysis data sets also involve a forced water balance closure by assuming a zero long-term storage change ($\Delta S = 0$ is applied over 23 years in Pan et al., 2012, and over 27 years in Zhang et al., 2018, across global catchments/grid-boxes). Despite the widespread applications, our results show that the "time scale" for assuming a negligible storage change remains elusive. Our results also suggest that the often adopted 5- or 10-year period in some previous studies may not be sufficiently long to satisfy the negligible storage change assumption, especially in arid and semiarid regions. When estimating E, a 5-year period could effectively limit e_{wb} to within ~10% (Figure 9k), whereas for estimating Q, 10 years seems to be the minimum period for humid and subhumid catchments (with e_{wb}/Q smaller than ~10%; Figure 9h). In arid and semiarid regions, a much longer period is required.

There are also limitations in the current study. One obvious limitation is data uncertainty, particularly uncertainties in the global P and E data sets. Here we use the MSWEP Version 2 global P data set, which represents an optimal combination of the highest quality P data sources available as a function of time scale and location (Beck et al., 2019). A recent evaluation study confirmed that the MSWEP global P data set generally exhibits the best performance against in situ observations among 22 global P data sets that are publicly available (Beck et al., 2017). For E, we started with four independent E estimates from global databases that were constructed without an explicit/implicit steady-state assumption. We then exclude the one E estimate that is most different from the other three for each catchment to further reduce the uncertainty in E estimates. Moreover, the difference in τ_s quantified using the four E estimates is generally small (Figure 3), suggesting that uncertainty in E estimates is unlikely to substantially change the findings. In addition, the observed Q is also subject to uncertainty (Di Baldassarre & Montanari, 2009). Nevertheless, the observed Q is the best available Q, which is also used for water balance calculation in other studies. In this light,

the findings and conclusions made here are valid and relevant for studies conducting catchment-based water balance calculations.

5. Conclusions

In this study, the utility of the steady-state assumption (negligible storage change) for water balance calculations is assessed using a combination of observed streamflow and precipitation and satellite/machine learning-based evapotranspiration estimates across 1,057 unimpaired catchments globally. The time that a catchment requires to reach the steady state (τ_s) is determined, the climate factors and surface properties that affect τ_s are investigated, and the associated error in water balance calculation when ignoring storage change is examined. The main conclusions are as follows:

1. Under the strictest criteria (i.e., ΔS^* %3C0.05 $\times \overline{P}$), about 71% of catchments reach steady state within 10 years, 53% of catchments reach steady state within 5 years, and ~6% of catchments fail to reach steady state within 30 years. We conclude that the actual τ_s is often longer than the conventionally assumed 5–10 years in many previous studies;
2. τ_s shows a statistically significant positive relationship with climate dryness and a negative relationship with NDVI, with arid/semiarid catchments as well as those with low vegetation cover generally requiring a longer time to reach a quasi-steady state. In addition, catchments with higher snowfall fraction are also found to have longer τ_s;
3. Imbalance in catchment water balance calculations resulting from the steady-state assumption increases as the time scale used for the water balance calculation decreases. For estimating E, a typical 5- to 10-year period would effectively limit the error (e_{wb}/E) within ~10% for most catchments. However, for estimating Q, a 10-year period would still be sufficient for catchments in humid and subhumid regions (yielding an e_{wb}/Q of less than 10%) but is too short for catchments in more arid regions.

Data Availability Statement

All data for this paper are properly cited and referred to in the reference list. Specifically, observed steamflow data are available from Lehner (2012), Falcone et al. (2010), and Zhang et al. (2013) (and in http://www.snirh.gov.br/hidroweb, https://www.canada.ca/en/environment-climate-change, and http://www.cr2.cl/datos-de-caudales/). Precipitation, air temperature, and potential evapotranspiration are available from Beck et al. (2019), Weedon et al. (2014) and Harris et al. (2014), respectively. The four global E estimates are available from Zhang, Yang, et al. (2016), Zhang et al. (2015), Martens et al. (2017), and Jung et al. (2011). Soil water holding capacity data are available from the Global Soil Data Task Group (2000), and NDVI data are available from Pinzon and Tucker (2014).

Acknowledgments

This study is financially supported by the National Natural Science Foundation of China (Grant 41890821), the Ministry of Science and Technology of China (Grant 2019YFC1510604), the Qinghai Department of Science and Technology (Grant 2019-SF-A4), and the Guoqiang Institute of Tsinghua University (Grant 2019GQG1020). M. L. Roderick and T. R. McVicar acknowledge support from the Australian Research Council (CE170100023). The following organizations are thanked for providing observed streamflow data: the U.S. Geological Survey (USGS), the Global Runoff Data Centre (GRDC), the Brazilian Brazilian Agência Nacional de Águas, the Water Survey of Canada (WSC), the Australian Bureau of Meteorology (BoM), and the Chilean Chilean Center for Climate and Resilience Research (CR2). We thank Ryan E. Emanuel and two other anonymous reviewers, and WRR Editors, for helpful comments that improved this research.

References

Abatzoglou, J. T., & Ficklin, D. L. (2017). Climatic and physiographic controls of spatial variability in surface water balance over the contiguous United States using the Budyko relationship. *Water Resources Research*, *53*, 7630–7643. https://doi.org/10.1002/2017WR020843

Anderegg, W. R. L., Klein, T., Bartlett, M., Sack, L., Pellegrini, A. F. A., Choat, B., & Jansen, S. (2016). Meta-analysis reveals that hydraulic traits explain cross-species patterns of drought-induced tree mortality across the globe. *Proceedings of the National Academy of Sciences*, *113*(18), 5024–5029. https://doi.org/10.1073/pnas.1525678113

Andréassian, V., & Perrin, C. (2012). On the ambiguous interpretation of the Turc-Budyko nondimensional graph. *Water Resources Research*, *48*, W10601. https://doi.org/10.1029/2012WR012532

Beck, H. E., de Roo, A., & van Dijk, A. I. J. M. (2015). Global maps of streamflow charactieristics based on observations from several thousand catchments. *Journal of Hydrometeorology*, *16*(4), 1478–1501. https://doi.org/10.1175/JHM-D-14-0155.1

Beck, H. E., Vergopolan, N., Pan, M., Levizzani, V., & Wood, E. F. (2017). Global-scale evaluation of 22 precipitation datasets using gauge observations and hydrological modeling. *Hydrology and Earth System Sciences*, *21*(12), 6201–6217. https://doi.org/10.5194/hess-21-6201-2017

Beck, H. E., Wood, E. F., Pan, M., Fisher, C. K., Miralles, D. G., van Dijk, A. I. J. M., et al. (2019). MSWEP V2 global 3-hourly 0.1° precipitation: Methodology and quantitative assessment. *Bulletin of the American Meteorological Society*, *100*(3), 473–500. https://doi.org/10.1175/BAMS-D-17-0138.1

Berghuijs, W. R., Woods, R. A., & Hrachowitz, M. (2014). A precipitation shift from snow towards rain leads to a decrease in streamflow. *Nature Climate Change*, *4*(7), 583–586. https://doi.org/10.1038/nclimate2246

Budyko, M. I., Miller, D. H., & Miller, D. H. (1974). *Climate and life*. New York: Academic press.

Choudhury, B. J. (1999). Evaluation of an empirical equation for annual evaporation using field observations and results from a biophysical model. *Journal of Hydrology*, *216*(1–2), 99–110. https://doi.org/10.1016/S0022-1694(98)00293-5

Daly, E., Calabrese, S., Yin, J., & Porporato, A. (2019). Hydrological spaces of long-term catchment water balance. *Water Resources Research*, *55*, 10,747–10,764. https://doi.org/10.1029/2019WR025952

Di Baldassarre, G., & Montanari, A. (2009). Uncertainty in river discharge observations: A quantitative analysis. *Hydrology and Earth System Sciences*, *13*(6), 913–921. https://doi.org/10.5194/hess-13-913-2009

Donohue, R. J., Roderick, M., & McVicar, T. R. (2007). On the importance of including vegetation dynamics in Budyko's hydrological model. *Hydrology and Earth System Sciences*, *11*(2), 983–995. https://doi.org/10.5194/hess-11-983-2007

Donohue, R. J., Roderick, M., & McVicar, T. R. (2010). Can dynamic vegetation information improve the accuracy of Budyko's hydrological model? *Journal of Hydrology*, *390*(1–2), 23–34. https://doi.org/10.1016/j.jhydrol.2010.06.025

Donohue, R. J., Roderick, M., & Mcvicar, T. R. (2012). Roots, storms and soil pores: Incorporating key ecohydrological processes into Budyko's hydrological model. *Journal of Hydrology*, *436-437*, 35–50. https://doi.org/10.1016/j.jhydrol.2012.02.033

Emanuel, R. E., D'Odorico, P., & Epstein, H. E. (2007). Evidence of optimal water use by vegetation across a range of North American ecosystems. *Geophysical Research Letters*, *34*, L07401. https://doi.org/10.1029/2006GL028909

Emanuel, R. E., Hazen, A. G., McGlynn, B. L., & Jencso, K. G. (2014). Vegetation and topographic influences on the connectivity of shallow groundwater between hillslopes and streams. *Ecohydrology*, *7*(2), 887–895. https://doi.org/10.1002/eco.1409

Evans, J. P., & Jakeman, A. (1998). Development of a simple, catchment-scale, rainfall-evapotranspiration-runoff model. *Environmental Modelling & Software*, *13*(3–4), 385–393. https://doi.org/10.1016/S1364-8152(98)00043-7

Falcone, J. A., Carlisle, D. M., Wolock, D. M., & Meador, M. R. (2010). GAGES: A stream gage database for evaluating natural and altered flow conditions in the conterminous United States. *Ecology*, *91*(2), 621–621. https://doi.org/10.1890/09-0889.1

Farmer, D., Sivapalan, M., & Jothityangkoon, C. (2003). Climate, soil, and vegetation controls upon the variability of water balance in temperate and semiarid landscapes: Downward approach to water balance analysis. *Water Resources Research*, *39*(2), 1035. https://doi.org/10.1029/2001WR000328

Flerchinger, G. N., & Cooley, K. R. (2000). A ten-year water balance of a mountainous semi-arid watershed. *Journal of Hydrology*, *237*(1–2), 86–99. https://doi.org/10.1016/S0022-1694(00)00299-7

Greve, P., Gudmundsson, L., Orlowsky, B., & Seneviratne, S. I. (2016). A two-parameter Budyko function to represent conditions under which evapotranspiration exceeds precipitation. *Hydrology and Earth System Sciences*, *20*(6), 2195–2205. https://doi.org/10.5194/hess-20-2195-2016

Harman, C. J., Troch, P. A., & Sivapalan, M. (2011). Functional model of water balance variability at the catchment scale: 2. Elasticity of fast and slow runoff components to precipitation change in the continental United States. *Water Resources Research*, *47*, W02523. https://doi.org/10.1029/2010WR009656

Harris, I., Jones, P. D., Osborn, T. J., & Lister, D. H. (2014). Updated high-resolution grids of monthly climatic observations—The CRU TS3.10 Dataset. *International Journal of Climatology*, *34*(3), 623–642. https://doi.org/10.1002/joc.3711

Istanbulluoglu, E., Wang, T., Wright, O. M., & Lenters, J. D. (2012). Interpretation of hydrologic trends from a water balance perspective: The role of groundwater storage in the Budyko hypothesis. *Water Resources Research*, *48*, W00H16. https://doi.org/10.1029/2010WR010100

Jung, M., Reichstein, M., Margolis, H. A., Cescatti, A., Richardson, A. D., Arain, M. A., et al. (2011). Global patterns of land-atmosphere fluxes of carbon dioxide, latent heat, and sensible heat derived from eddy covariance, satellite, and meteorological observations. *Journal of Geophysical Research*, *116*, G00J07. https://doi.org/10.1029/2010JG001566

Koster, R. D., & Suarez, M. J. (1999). A simple framework for examining the interannual variability of land surface moisture fluxes. *Journal of Climate*, *12*(7), 1911–1917. https://doi.org/10.1175/1520-0442(1999)012%3C1911:ASFFET%3E2.0.CO;2

Le Houérou, H. N., Bingham, R. L., & Skerbek, W. (1988). Relationship between the variability of primary production and the variability of annual precipitation in world arid lands. *Journal of Arid Environments*, *15*(1), 1–18. https://doi.org/10.1016/S0140-1963(18)31001-2

Lehner, B. (2012). *Derivation of watershed boundaries for GRDC gauging stations based on the HydroSHEDS drainage network* (Vol. 41, p. 12) Montreal, Canada: Federal Institute of Hydrology (BfG) Global Runoff Data Centre Tech. Rep. https://www.bafg.de/GRDC/EN/02_srvcs/24_rprtsrs/report_41.pdf?__blob=publicationFile

Lehner, B., Liermann, C. R., Revenga, C., Vörösmarty, C., Fekete, B., Crouzet, P., et al. (2011). High-resolution mapping of the world's reservoirs and dams for sustainable river-flow management. *Frontiers in Ecology and the Environment*, *9*(9), 494–502. https://doi.org/10.1890/100125

Li, D., Pan, M., Cong, Z., Zhang, L., & Wood, E. (2013). Vegetation control on water and energy balance within the Budyko framework. *Water Resources Research*, *49*, 969–976. https://doi.org/10.1002/wrcr.20107

Li, L. J., Zhang, L., Wang, H., Wang, J., Yang, J. W., Jiang, D. J., et al. (2007). Assessing the impact of climate variability and human activities on streamflow from the Wuding River basin in China. *Hydrological Processes*, *21*(25), 3485–3491. https://doi.org/10.1002/hyp.6485

Liang, W., Bai, D., Wang, F., Fu, B., Yan, J., Wang, S., et al. (2015). Quantifying the impacts of climate change and ecological restoration on streamflow changes based on a Budyko hydrological model in China's Loess Plateau. *Water Resources Research*, *51*, 6500–6519. https://doi.org/10.1002/2014WR016589

Liu, J., Zhang, Q., Feng, S., Gu, X., Singh, V. P., & Sun, P. (2019). Global attribution of runoff variance across multiple timescales. *Journal of Geophysical Research: Atmospheres*, *124*, 13,962–13,974. https://doi.org/10.1029/2019JD030539

Llorens, P., & Domingo, F. (2007). Rainfall partitioning by vegetation under Mediterranean conditions: A review of studies in Europe. *Journal of Hydrology*, *335*(1–2), 37–54. https://doi.org/10.1016/j.jhydrol.2006.10.032

Martens, B., Gonzalez Miralles, D., Lievens, H., Van Der Schalie, R., De Jeu, R. A., Fernández-Prieto, D., et al. (2017). GLEAM v3: Satellite-based land evaporation and root-zone soil moisture. *Geoscientific Model Development*, *10*(5), 1903–1925. https://doi.org/10.5194/gmd-10-1903-2017

McVicar, T. R., Roderick, M. L., Donohue, R. J., & Van Niel, T. G. (2012). Less bluster ahead? Ecohydrological implications of global trends of terrestrial near-surface wind speeds. *Ecohydrology*, *5*(4), 381–388. https://doi.org/10.1002/eco.1298

Milly, P. C. D. (1994). Climate, soil water storage, and the average annual water balance. *Water Resources Research*, *30*(7), 2143–2156. https://doi.org/10.1029/94WR00586

Milly, P. C. D., & Dunne, K. A. (2002). Macroscale water fluxes 2. Water and energy supply control of their interannual variability. *Water Resources Research*, *38*(10), 1206. https://doi.org/10.1029/2001WR000760

Miralles, D., Holmes, T., De Jeu, R., Gash, J., Meesters, A., & Dolman, A. (2011). Global land-surface evaporation estimated from satellite-based observations. *Hydrology and Earth System Sciences*, *12*(2), 453–469. https://doi.org/10.5194/hess-15-453-2011

Monteverdi, J. P. (1976). The single air mass disturbance and precipitation characteristics at San Francisco. *Monthly Weather Review*, *104*(10), 1289–1296. https://doi.org/10.1175/1520-0493(1976)104%3C1289:TSAMDA%3E2.0.CO;2

Nippgen, F., McGlynn, B. L., & Emanuel, R. E. (2015). The spatial and temporal evolution of contributing areas. *Water Resources Research*, *51*, 4550–4573. https://doi.org/10.1002/2014WR016719

Nippgen, F., McGlynn, B. L., Emanuel, R. E., & Vose, J. M. (2016). Watershed memory at the Coweeta Hydrologic Laboratory: The effect of past precipitation and storage on hydrologic response. *Water Resources Research*, *52*, 1673–1695. https://doi.org/10.1002/2015WR018196

Pan, M., Sahoo, A. K., Troy, T. J., Vinukollu, R. K., Sheffield, J., & Wood, E. F. (2012). Multisource estimation of long-term terrestrial water budget for major global river basins. *Journal of Climate*, *25*(9), 3191–3206. https://doi.org/10.1175/JCLI-D-11-00300.1

Peel, M. C., McMahon, T. A., & Finlayson, B. L. (2010). Vegetation impact on mean annual evapotranspiration at a global catchment scale. *Water Resources Research*, *46*, W09508. https://doi.org/10.1029/2009WR008233

Pinzon, J., & Tucker, C. (2014). A non-stationary 1981–2012 AVHRR NDVI3g time series. *Remote Sensing*, *6*(8), 6929–6960. https://doi.org/10.3390/rs6086929

Potter, N. J., & Zhang, L. (2009). Interannual variability of catchment water balance in Australia. *Journal of Hydrology*, *369*(1–2), 120–129. https://doi.org/10.1016/j.jhydrol.2009.02.005

Potter, N. J., Zhang, L., Milly, P. C. D., McMahon, T. A., & Jakeman, A. J. (2005). Effects of rainfall seasonality and soil moisture capacity on mean annual water balance for Australian catchments. *Water Resources Research*, *41*, W06007. https://doi.org/10.1029/2004WR003697

Rice, J. S., & Emanuel, R. E. (2019). Ecohydrology of interannual changes in watershed storage. *Water Resources Research*, *55*, 8238–8251. https://doi.org/10.1029/2019WR025164

Roderick, M., Sun, F., Lim, W. H., & Farquhar, G. (2014). A general framework for understanding the response of the water cycle to global warming over land and ocean. *Hydrology and Earth System Sciences*, *18*(5), 1575–1589. https://doi.org/10.5194/hess-18-1575-2014

Roderick, M. L., & Farquhar, G. D. (2011). A simple framework for relating variations in runoff to variations in climatic conditions and catchment properties. *Water Resources Research*, *47*, W00G07. https://doi.org/10.1029/2010WR009826

Siebert, S., Kummu, M., Porkka, M., Döll, P., Ramankutty, N., & Scanlon, B. R. (2015). A global data set of the extent of irrigated land from 1900 to 2005. *Hydrology and Earth System Sciences*, *19*(3), 1521–1545. https://doi.org/10.5194/hess-19-1521-2015

Ukkola, A. M., & Prentice, I. J. H. (2013). A worldwide analysis of trends in water-balance evapotranspiration. *Hydrology and Earth System Sciences*, *17*(10), 4177–4187. https://doi.org/10.5194/hess-17-4177-2013

Wang, D. (2012). Evaluating interannual water storage changes at watersheds in Illinois based on long-term soil moisture and groundwater level data. *Water Resources Research*, *48*, W03502. https://doi.org/10.1029/2011WR010759

Wang, D., & Alimohammadi, N. (2012). Responses of annual runoff, evaporation, and storage change to climate variability at the watershed scale. *Water Resources Research*, *48*, W05546. https://doi.org/10.1029/2011WR011444

Wang, L., Good, S. P., & Caylor, K. K. (2014). Global synthesis of vegetation control on evapotranspiration partitioning. *Geophysical Research Letters*, *41*, 6753–6757. https://doi.org/10.1002/2014GL061439

Wang, T., Istanbulluoglu, R., Lenters, J., & Scott, D. (2009). On the role of groundwater and soil texture in the regional water balance: An investigation of the Nebraska Sand Hills, USA. *Water Resources Research*, *45*, W10413. https://doi.org/10.1029/2009WR007733

Weedon, G. P., Balsamo, G., Bellouin, N., Gomes, S., Best, M. J., & Viterbo, P. (2014). The WFDEI meteorological forcing data set: WATCH Forcing Data methodology applied to ERA-interim reanalysis data. *Water Resources Research*, *50*, 7505–7514. https://doi.org/10.1002/2014WR015638

Williams, C. A., & Albertson, J. D. (2005). Contrasting short-and long-timescale effects of vegetation dynamics on water and carbon fluxes in water-limited ecosystems. *Water Resources Research*, *41*, W06005. https://doi.org/10.1029/2004WR003750

Xue, B. L., Wang, L., Li, X., Yang, K., Chen, D., & Sun, L. (2013). Evaluation of evapotranspiration estimates for two river basins on the Tibetan Plateau by a water balance method. *Journal of Hydrology*, *492*, 290–297. https://doi.org/10.1016/j.jhydrol.2013.04.005

Yang, D., Shao, W., Yeh, P. J. F., Yang, H., Kanae, S., & Oki, T. (2009). Impact of vegetation coverage on regional water balance in the nonhumid regions of China. *Water Resources Research*, *45*, W00A14. https://doi.org/10.1029/2008WR006948

Yang, D., Sun, F., Liu, Z., Cong, Z., & Lei, Z. (2006). Interpreting the complementary relationship in non-humid environments based on the Budyko and Penman hypotheses. *Geophysical Research Letters*, *33*, L18402. https://doi.org/10.1029/2006GL027657

Yang, D., Sun, F., Liu, Z., Cong, Z., Ni, G., & Lei, Z. (2007). Analyzing spatial and temporal variability of annual water-energy balance in nonhumid regions of China using the Budyko hypothesis. *Water Resources Research*, *43*, W04426. https://doi.org/10.1029/2006WR005224

Yang, Y., Donohue, R. J., & McVicar, T. R. (2016). Global estimation of effective plant rooting depth: Implications for hydrological modeling. *Water Resources Research*, *52*, 8260–8276. https://doi.org/10.1002/2016WR019392

Yang, Y., Donohue, R. J., McVicar, T. R., & Roderick, M. L. (2015). An analytical model for relating global terrestrial carbon assimilation with climate and surface conditions using a rate limitation framework. *Geophysical Research Letters*, *42*, 9825–9835. https://doi.org/10.1002/2015gl066835

Yang, Y., Donohue, R. J., McVicar, T. R., Roderick, M. L., & Beck, H. E. (2016). Long-term CO_2 fertilization increases vegetation productivity and has little effect on hydrological partitioning in tropical rainforests. *Journal of Geophysical Research: Biogeosciences*, *121*, 2125–2140. https://doi.org/10.1002/2016JG003475

Yang, Y., Long, D., Guan, H., Scanlon, B. R., Simmons, C. T., Jiang, L., & Xu, X. (2014). GRACE satellite observed hydrological controls on interannual and seasonal variability in surface greenness over mainland Australia. *Journal of Geophysical Research: Biogeosciences*, *119*, 2245–2260. https://doi.org/10.1002/2014JG002670

Yang, Y., McVicar, T. R., Donohue, R. J., Zhang, Y., Roderick, M. L., Chiew, F. H., et al. (2017). Lags in hydrologic recovery following an extreme drought: Assessing the roles of climate and catchment characteristics. *Water Resources Research*, *53*, 4821–4837. https://doi.org/10.1002/2017WR020683

Yin, D., & Roderick, M. L. (2020). Inter-annual variability of the global terrestrial water cycle. *Hydrology and Earth System Sciences*, *24*(1), 381–396. https://doi.org/10.5194/hess-24-381-2020

Yokoo, Y., Sivapalan, M., & Oki, T. (2008). Investigating the roles of climate seasonality and landscape characteristics o n mean annual and monthly water balances. *Journal of Hydrology*, *357*(3–4), 255–269. https://doi.org/10.1016/j.jhydrol.2008.05.010

Zhang, K., Kimball, J. S., Nemani, R. R., Running, S. W., Hong, Y., Gourley, J. J., & Yu, Z. (2015). Vegetation greening and climate change promote multidecadal rises of global land evapotranspiration. *Scientific Reports*, *5*(1), 15956. https://doi.org/10.1038/srep15956

Zhang, L., Hickel, K., Dawes, W. R., Chiew, F. H. S., Western, A. W., & Briggs, P. R. (2004). A rational function approach for estimating mean annual evapotranspiration. *Water Resources Research*, *40*, W02502. https://doi.org/10.1029/2003WR002710

Zhang, Y., Pan, M., Sheffield, J., Siemann, A. L., Fisher, C. K., Liang, M., et al. (2018). A Climate Data Record (CDR) for the global terrestrial water budget: 1984–2010. *Hydrology and Earth System Sciences*, *22*(1), 241–263. https://doi.org/10.5194/hess-22-241-2018

Zhang, L., Potter, N., Hickel, K., Zhang, Y., & Shao, Q. (2008). Water balance modeling over variable time scales based on the Budyko framework—Model development and testing. *Journal of Hydrology*, *360*(1–4), 117–131. https://doi.org/10.1016/j.jhydrol.2008.07.021

Zhang, S., Yang, H., Yang, D., & Jayawardena, A. W. (2016). Quantifying the effect of vegetation change on the regional water balance within the Budyko framework. *Geophysical Research Letters*, *43*, 1140–1148. https://doi.org/10.1002/2015GL066952

Zhang, Y., Viney, N., Frost, A., Oke, A., Brooks, M., Chen, Y., & Campbell, N. (2013). *Collation of Australian modeller's streamflow dataset for 780 unregulated Australian catchments* (pp. 1–115). Canberra, Australia: CSIRO: Water for a Healthy Country National Research Flagship.